Optical Engineering

OpticalEngineering.SPIEDigitalLibrary.org

Angle of linear polarization images of outdoor scenes

Meredith Kupinski
Christine Bradley
David Diner
Feng Xu
Russell Chipman

SPIE.

Meredith Kupinski, Christine Bradley, David Diner, Feng Xu, Russell Chipman, "Angle of linear polarization images of outdoor scenes," *Opt. Eng.* **58**(8), 082419 (2019), doi: 10.1117/1.OE.58.8.082419.

Angle of linear polarization images of outdoor scenes

Meredith Kupinski,[a,*] Christine Bradley,[b] David Diner,[b] Feng Xu,[b] and Russell Chipman[a]
[a]University of Arizona, College of Optical Sciences, Tucson, Arizona, United States
[b]California Institute of Technology, Jet Propulsion Laboratory, Pasadena, California, United States

Abstract. Observations from the Ground-based Multiangle SpectroPolarimetric Imager (GroundMSPI) are used to relate angle of linear polarization (AoLP) measurements to material properties and illumination conditions in sunlit outdoor environments. GroundMSPI is a push-broom spectropolarimetric camera with an uncertainty in degree of linear polarization (DoLP) of ± 0.005. This polarimetric accuracy yields useful AoLP images even when the DoLP is less than 0.02. AoLP images are reported with respect to dependency on surface texture, surface orientation, albedo, and illumination conditions. Agreement with well-known principles of polarized light scattering is illustrated, and several special cases are described. Expected observations of AoLP tangential to surface orientation and AoLP perpendicular to the scattering plane are reported. Significant changes in the AoLP are observed from common variations in outdoor illumination conditions. Also, simple variants in material properties change the dominant polarized light scattering process and thus the AoLP. Measurement examples that isolate a 90 deg AoLP flip are shown for a sunny and cloudy day as well as an object of high and low albedo. [DOI: 10.1117/1.OE.58.8.082419]

Keywords: angle of linear polarization; polarimetric imaging; polarized light scattering; multiangle spectropolarimetric imager.

Paper 181738SS received Dec. 3, 2018; accepted for publication May 20, 2019; published online Jun. 11, 2019; corrected Oct. 7, 2021.

1 Introduction

Directly transmitted sunlight incident upon the Earth's surface is almost completely unpolarized and becomes partially polarized when reflected from natural or man-made materials.[1] The measured degree of polarization of solar-illuminated outdoor scenes is typically under 0.10 and even more commonly under 0.05 for natural materials such as foliage or soil. Much larger polarization in sunlit scenes generally results from specular reflection from metals or bodies of water where, depending upon the scattering angle, the degree of polarization can reach 0.50 to 0.60. In addition, polarimetry can capture the signatures of objects illuminated by diffuse skylight (either due to being in shadow or in the presence of overcast skies), and nonmetallic rough surfaces have polarization signatures in off-specular directions.[2] The characteristics of polarized light scattered from the Earth's surface is highly dependent upon the interplay of sunlight, atmospheric conditions, and the material properties of the illuminated scenes. For a majority of cases, this interplay is complicated. Even a rudimentary analysis of Stokes images requires *a priori* knowledge of the scene conditions to select and test polarimetric models and expected trends. The images in this paper are selected to show simple scene conditions with each factor as isolated as possible. These selections are useful demonstrations of the most significant scene variables' effect on polarimetric light scattering.

The majority of research into the polarimetric properties of illuminated scenes at visible and near-infrared wavelengths is concerned with the degree of linear polarization (DoLP). Less well studied is the angle of linear polarization (AoLP), which contains additional information relating to material properties and illumination conditions.[3] In this paper, Ground-based Multiangle SpectroPolarimetric Imager (GroundMSPI)[4] observations of sunlit scenes containing grass, foliage, buildings, man-made structures, and roads are analyzed. GroundMSPI AoLP images are discussed in the context of well-known principles of polarized light scattering and prior observations by other researchers.[1,5,6] The novelty of this work is the study of AoLP using a high-accuracy imaging polarimeter. GroundMSPI is designed to provide a ± 0.005 DoLP uncertainty. This high measurement quality yields accurate AoLP information even when the DoLP is <0.02.[7] Images in this paper are selected from three years of GroundMSPI data collection. Representative samples from this diverse dataset provide demonstrations of polarized light scattering in a wide range of environmental conditions. This study is motivated by a need for accurate modeling of the polarized light scattering of the Earth's surface for passive retrievals of atmospheric aerosol properties from downward-looking observations.

2 Related Work

GroundMSPI is an early prototype for an aircraft and satellite instrument to measure multiangle multispectral imaging polarization from above the top of the atmosphere. The Airborne Multiangle SpectroPolarimetric Imager (AirMSPI) is the next in the sequence of prototypes and has participated in several NASA field campaigns.[8,9] The MSPI camera architecture uses a time-varying retardance in the optical path to modulate the orientation of the linearly polarized component of the incoming light, described by the Stokes components Q (excess of horizontally over vertically oriented polarized light) and U (excess of 45 deg over 135 deg oriented polarized light). Modulation of Q and U over a wide spectral range is obtained using a pair of quarter-wave plates, a pair of photoelastic modulators, and a high-speed push-broom detector array.[4,8] Retardance is within 8 deg of quarter wave at 470, 660, and 865 nm to yield measurements of

*Address all correspondence to Meredith Kupinski, E-mail: meredith@optics.arizona.edu

linear Stokes parameters at these three wavebands.[10] The departure from ideal performance is compensated in calibration. This architecture has been extended into the shortwave infrared with a second-generation aircraft instrument (AirMSPI-2) and is also utilized in the Multi-Angle Imager for Aerosols (MAIA) instrument, currently in development to study airborne particulate matter from space.[11] A recommendation by the Aerosol, Cloud and Ecosystems (ACE) working group for a multiangle multispectral polarimetric imager has motivated the development of these instruments.[12]

GroundMSPI has been deployed at the University of Arizona (UA) as a tool to measure and analyze land surface polarized reflectance to improve our understanding of the surface boundary condition for remotely sensed atmospheric aerosol retrievals.[10] Prior GroundMSPI analysis includes verifying region types for which the polarized bidirectional reflectance distribution function (p-BRDF) is spectrally invariant,[13] studying the error of AoLP measurements,[7] quantifying the spatial statistics of polarization images,[14] and modeling p-BRDF.[10,15,16]

The AoLP of the sky, and the associated dependency on cloud cover, has been discussed in several papers.[17–22] In this paper, we focus on the utility of AoLP for characterization of surface objects. It is the most extensive report, to our knowledge, of AoLP images of land surfaces and is organized as follows. In Sec. 3, definitions of terms and explanations of GroundMSPI AoLP and DoLP image renderings are presented. In Sec. 4, GroundMSPI AoLP images are categorized according to the studies of: (A) surface texture and orientation, (B) albedo, and (C) illumination conditions. In each case corresponding DoLP images are also reported. Section 5 presents conclusions and future work.

3 Terminology and Methods

The Stokes parameters uniquely quantify the polarization state of incoherent light with four numbers, denoted as $[I, Q, U, V]$.[23] The first component I represents the total radiance, and the other components also have units of radiance. The definitions of Q and U must be associated with a coordinate system, usually either the scattering or meridian planes (see Fig. 12 in Sec. 6). Circular polarization V is typically negligible for sunlight scattered by the atmosphere or Earth's surface[24] and is not measured by GroundMSPI. The linear Stokes components are often combined into a dimensionless quantity, the DoLP, which is expressed as

$$\mathrm{DoLP} = \frac{\sqrt{Q^2 + U^2}}{I} = \frac{I_{\mathrm{pol}}}{I} = \sqrt{q^2 + u^2}, \tag{1}$$

where I_{pol} is the polarized radiance (the fraction of light in the scene that is polarized) and $q = Q/I$ and $u = U/I$. The AoLP is expressed as

$$\mathrm{AoLP} = \frac{1}{2}\tan^{-1}\left(\frac{U}{Q}\right) = \frac{1}{2}\tan^{-1}\left(\frac{u}{q}\right). \tag{2}$$

Note that DoLP and radiance measurements are invariant to the coordinate system of Q and U, but AoLP depends on the coordinate system. Equations (1) and (2) are operational definitions. GroundMSPI uses a photoelastic-modulator-based polarimetric imaging technique to measure I, Q, and U in three wavebands (470, 660, and 865 nm) with an uncertainty in DoLP of ± 0.005.[4] This polarimetric accuracy yields useful AoLP images even when the DoLP is <0.02[7].

A color map that designates unique hues in the range 0 deg to 180 deg is used to render AoLP images. This color map is displayed on a circle so that the hue in an AoLP image can be visually matched to an orientation. Coordinate systems and circular color-mapping conventions are detailed in Fig. 12 of Sec. 6. For the remainder of the paper AoLP_m and AoLP_s will denote AoLP reported in meridian and scattering coordinates, respectively.

A fusion of DoLP and AoLP is often created to visually convey the three-dimensional linear Stokes parameters simultaneously.[25] Analyzing the AoLP independently offers the simplicity of reconciling this scalar value with an expected value based on prior knowledge of polarized light scattering phenomenon. Also, the spatial statistics of AoLP offers a practical way to test the fidelity of the polarimetric signature. If the spatial variation of AoLP is high in a given region, i.e., a noisy appearance in the AoLP image, then the polarimetric signal is smaller than the measurement capability of the instrument. Alternatively, a homogenous region in an AoLP image, or a region that varies with an expected trend, conveys confidence in the measurement fidelity. The MSPI modulation technique has been developed to measure the normalized Stokes parameters q and u with high accuracy; hence, DoLP and AoLP, which are functions of these quantities [see Eqs. (1) and (2)] are also highly accurate. GroundMSPI AoLP images reveal high confidence in a variety of polarimetric measurements even in the shade and for highly depolarizing materials. When the DoLP is 0.02, the standard deviation in the AoLP is about 6 deg, assuming normally distributed linear Stokes vectors with a standard deviation of 0.005.[7]

Table 1 in Sec. 6 reports date, time, location, and view geometry for all GroundMSPI datasets in this paper.

Table 1 GroundMSPI image acquisition details.

Figure	Date	Time	Location	View direction
1,2	April 10, 2015	11:30 MST	32°13′N–110°56′W	N
3	April 13, 2015	12:30 MST	32°13′N–110°56′W	NW
4	April 13, 2015	10:46, 12:30, 14:05 MST	32°13′N–110°56′W	NW
5	April 05, 2015	11:34 MST	32°20′N–110°53′W	S
6	July 22, 2015	8:15 MST	32°19′N–110°55′W	W
8	June 19, 2015	9:34 MST	32°14′N–110°52′W	SW
9	June 08, 2015	14:50 MST	32°13′N–110°56′W	E
10	April 01, 2015	15:52 MST	32°13′N–110°56′W	E
11	July 22, 2015	16:18 MST	32°19′N–110°55′W	N

4 GroundMSPI observations

4.1 *Relationship of Angle of Linear Polarization to Surface Texture and Orientation*

Matching the sky AoLP to expectations is an informative way to start GroundMSPI AoLP image analysis. The AoLP of a cloudless sky can be described by a single-scattering Rayleigh model where the polarization orientation is 90 deg from the scattering plane.[19] When reporting AoLP images, the effect being demonstrated dictates which coordinate system is most insightful. For comparison, Fig. 1 shows a spring carnival on the UA campus in both scattering coordinates and meridian coordinates. At a given time the coordinate system can be readily identified from the color circle. When 0 deg AoLP is aligned with the zenith (i.e., the vertical direction of an image) the AoLP is reported in meridian coordinates and is denoted as AoLP_m. When 0 deg AoLP on the color circle is tilted away from vertical,

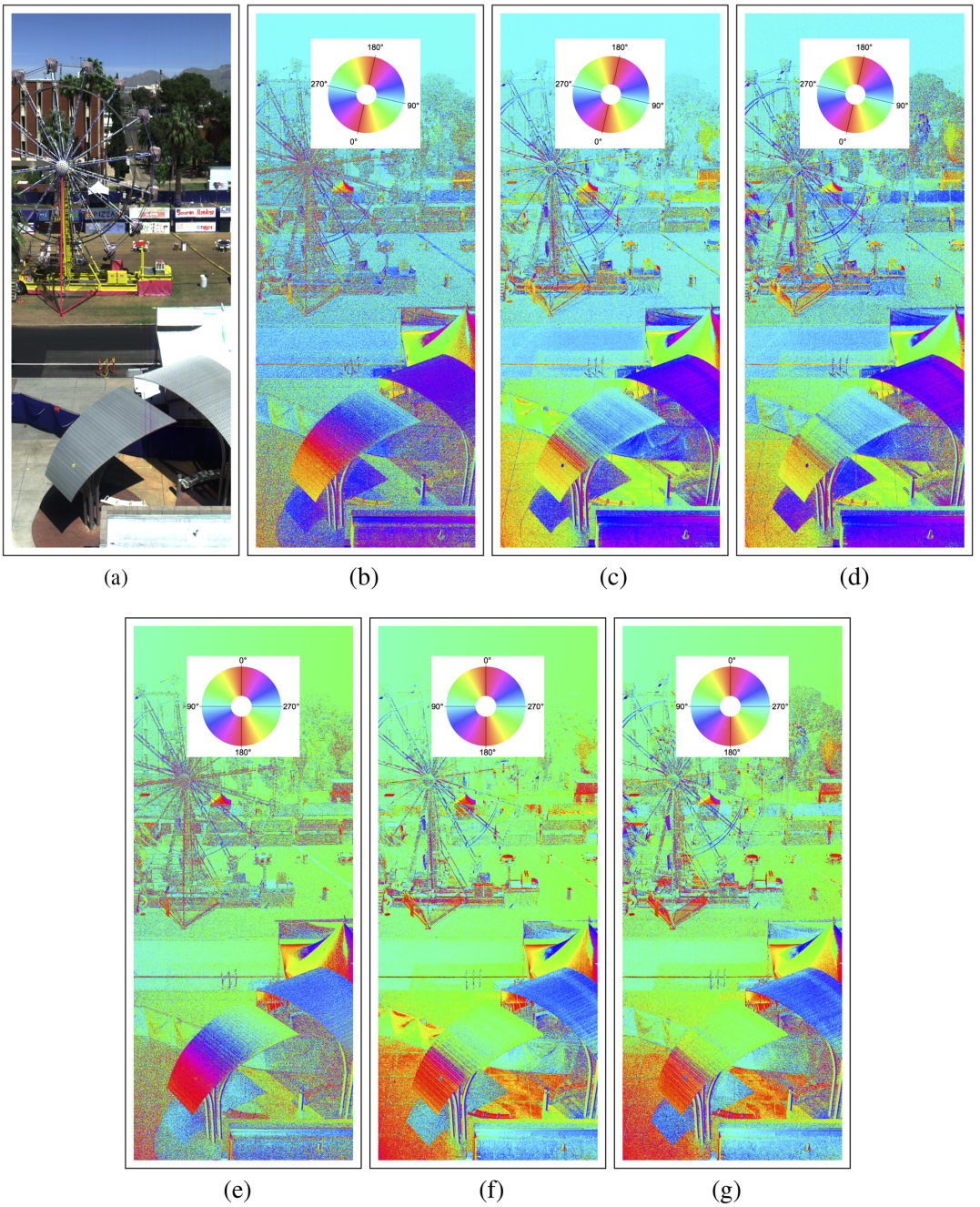

Fig. 1 Spring carnival in (a) RGB radiance, (b)–(d) AoLP_s images in scattering coordinates, and (e)–(g) AoLP_m images in meridian coordinates for 470, 660, and 865 nm, respectively. For natural materials and man-made materials, which are rough, AoLP measurements usually match a cloudless sky. This value is constant throughout the day in scattering coordinates and is rendered in cyan. This value changes throughout the day in meridian coordinates. Time-lapsed movies of AoLP_s and AoLP_m (08:03 to 16:36 MST) are provided [Video 1, 36 MB, MOV (URL: https://doi.org/10.1117/1.OE.58.8.082419.1) and Video 2, 35 MB, MOV (URL: https://doi.org/10.1117/1.OE.58.8.082419.2)].

the AoLP is reported in scattering coordinates and is denoted as AoLP_s.

At first glance, the AoLP_s images in Fig. 1 are mostly cyan, corresponding to an angle perpendicular to the scattering plane. The sky and the grass are cyan. The road is blue, which is about 95 deg. Polarized light scattering from natural surfaces such as vegetation and bare soil are modeled as single-scattering events oriented perpendicular to the scattering plane.[10,26] This prediction is based on a microfacet model of the p-BRDF, which describes the polarizance of a material as Fresnel reflections from subresolution-sized microfacets that are randomly oriented.[15,27] The plane of polarization for a cloudless sky is also expected to be perpendicular to the scattering plane, which is observed in GroundMSPI AoLP images.

As supplements to Fig. 1, two time-lapsed videos are provided for the scene shown. These videos show the progression of AoLP during the day (08:03 to 16:36 MST) at the three GroundMSPI polarimetric wavelengths, 470, 660, and 865 nm. The solar illumination direction changes throughout the day to provide a range of scattering angles with a constant view direction. The video of AoLP with respect to the scattering plane, AoLP_s (Video 1), shows the sky and roughened surfaces to be predominantly cyan throughout the day. Cyan indicates $\mathrm{AoLP}_s = 90$ deg. Also notice that the color circle rotates with time as the scattering plane changes with the varying solar illumination direction. The white tent and metal awnings in the foreground tend to deviate from $\mathrm{AoLP}_s = 90$ deg and the AoLP_s values are not constant throughout the day. Invariance of the AoLP to illumination angle can be readily identified in meridian coordinates.

The video corresponding to Fig. 1, panels (e)–(g), Video 2, shows the same scene with AoLP in meridian coordinates AoLP_m. Notice that the sky and rough surfaces (e.g., grass and soil) share the same AoLP at a given time. Throughout the day, the AoLP_m value of these objects changes. The rough (i.e., microfacet) surface model predicts that there will always be some set of microfacets that are at just the right orientation to specularly reflect sunlight into the camera, and therefore follow the prediction of Fresnel's laws in having polarization perpendicular to the scattering plane.

The meridian plane is defined by the view direction and zenith; it does not depend on the solar illumination direction and will remain constant when the view direction is constant. This reference frame allows for a useful look into smoother surface types such as the white tent and metal awnings. In particular, notice the white tent in the foreground. Once it is directly illuminated (after about 9 AM), the AoLP_m from most of the white tent in the foreground does not change with solar illumination angle and remains approximately perpendicular to the surface orientation. The exception to this trend is sun-specular reflections. Specular reflections are oriented 90 deg from the plane of incidence. The plane of incidence is defined by the illumination vector and the vector normal to the surface of the reflecting object. In the plane of incidence, the angle of incidence equals the angle of reflection for specular reflection. Therefore, when the view direction is aligned to a sun-specular reflection, the scattering plane equals the plane of incidence. The AoLP of sun-specular reflections is $\mathrm{AoLP}_s = 90$ deg and is rendered as cyan in scattering coordinates. Sun-specular reflections are saturated to white in the RGB image, which is difficult to identify on the white tent. The location of the sun-specular reflections is more obvious in the AoLP_s image; from 9:07 to 14:30 MST, a cyan sliver propagates across the right-side of the tent. For a given view and solar illumination geometry, there is a small range of surface orientations for which sun-specular reflections are observed. There is a white tent in the background that has the same AoLP trend but no sun-specular reflections are observed. The two metal shade awnings in the foreground exhibit an AoLP pattern similar to the white tents. At 8:41 MST, the awning on the right picks up sun-specular reflections for about 30 min. In off sun-specular directions the AoLP changes with the curvature of the metal awning and the angle of solar illumination until falling into the shade around 4:30 MST.

Figure 1 is the only dataset in this paper for which all three wavelengths of the same scene are shown. The AoLP is very similar within this wavelength range, with the notable exception that most regions appear noisier at 470 nm than at the two longer wavelengths. Also, there are a two notable objects for which the AoLP changes over the three wavelengths: the left side of the metal awning and the blue crowd-control barrier to the left of the awnings [see RGB radiance image in Fig. 1(a)]. Both of these objects also differ in DoLP, as can be seen in Fig. 2.

Figure 2 shows the DoLP at three different wavelengths for the same scene as Fig. 1. The DoLP of the sky changes by almost a factor of 2 over this wavelength range. This observation is within the variations reported by comprehensive sky polarization studies.[28] The highest DoLP object on the ground is the black road. Some color trends with DoLP are observed: the orange brick has a relatively higher DoLP at 470 nm and the DoLP of the blue crowd-control barrier at bottom-left of the image is highest at 660 nm. These trends match Umov's effect, which relates DoLP to albedo.[29]

To contrast rough and smooth materials, Fig. 3(a) displays both in a single scene: a smooth metal sculpture directly in front of a brick building under clear sky conditions. In the RGB image of Fig. 3(a), sun-specular reflections are observed on the top half of the statue's head and the shoulders. Figure 3(b) is a close-up of the spherical head of the metal statue and shows an AoLP that varies tangential to the surface on the bottom-half of the sphere and an AoLP that is 90° from the scattering plane for most of the top-half of the sphere. The top-half of the sphere are sun-specular reflections and the bottom-half of the sphere are specular reflections from the sky dome. In the shade of direct solar illumination, incident radiation comes from scattered skylight. Figure 3(b) shows the notable difference between sun-specular and sky-specular AoLP trends. On the bottom-half of the sphere for any given surface orientation and view geometry there is incident radiation from skylight illumination and the AoLP is perpendicular to the plane of incidence. Scattered skylight is an extended source illuminating from many angles. When both direct and skylight illumination are blocked in deep shade, such as the hole near the neck of the sculpture, the AoLP is noisy due to very low reflected polarized radiance.

Consistent with rough surface p-BRDF models, the AoLP of the cloudless sky is the same as the AoLP from the brick

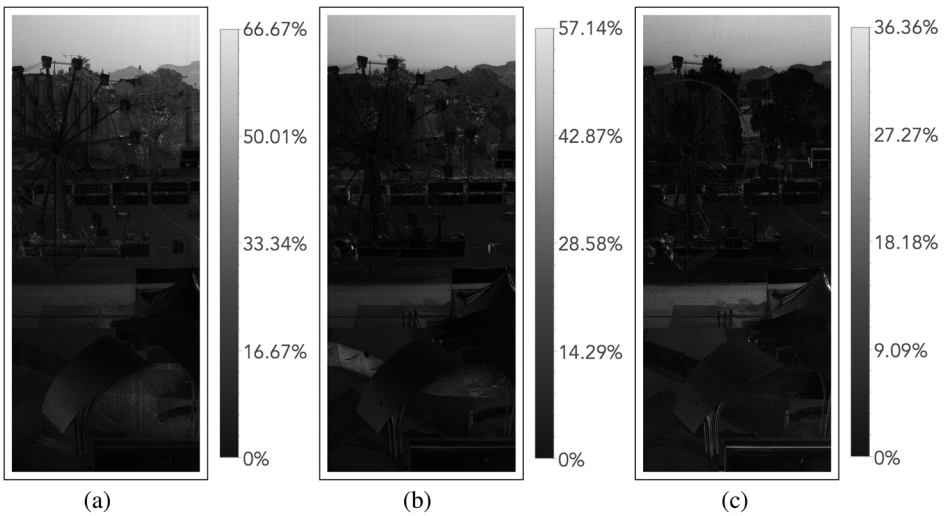

Fig. 2 Spring carnival in DoLP (a)–(c) for 470, 660, and 865 nm, respectively. Note that the DoLP of the sky is highest in 470 nm due to stronger Rayleigh scattering. A time-lapse DoLP movie (08:03 to 16:36 MST) is provided [Video 3, 21 MB, MOV (URL: https://doi.org/10.1117/1.OE.58.8.082419.3)].

building, gravel ground, and cement base of the statue when these objects are directly illuminated. Prior work demonstrated agreement between GroundMSPI measurements of directly solar-illuminated rough surfaces and a microfacet polarized light scattering model, which predicts the AoLP is always perpendicular to the scattering plane.[10] This p-BRDF model comprises a volumetric reflection term plus a specular reflection term of Fresnel-reflecting microfacets.[27]

Three measurements at different times are shown in Fig. 4. Note that the base of the statue is cement and the AoLP is nearly insensitive to surface orientation and closely matches the AoLP of the brick building. The rough surface AoLP changes with solar illumination angle and matches the AoLP of the cloudless sky, which is perpendicular to the scattering plane. In the locations of sun-specular reflections, the top-half of the head and the middle-left part of the shoulders, the AoLP matches rough surface scattering (i.e., perpendicular to the scattering plane). However, the bottom-half of the sculpture's head and the bottom of the sculpture's body maintain nearly the same AoLP that is tangential to the surface and invariant to different solar illumination angles. In the locations of sun-specular reflections, the top-half of the head and the middle-left part of the shoulders, the AoLP matches rough surface scattering (i.e., perpendicular to the scattering plane).

This tangential relationship between AoLP and surface orientation is not unique to metallics. As shown in Fig. 5, nonmetallic smooth surfaces can also exhibit AoLP that is either perpendicular to the scattering plane or tangential to the surface orientation. For a plastic trash can and recycling bin, the AoLP direction is superimposed on the cropped area in Fig. 5(b) and exhibits the tangential relationship. Similarly, the AoLP from the windshield of the car in Fig. 5 is tangential to the surface. On the other hand, the AoLP from the hood of the car is perpendicular to the surface. It is reasonable to classify both of these materials as smooth.

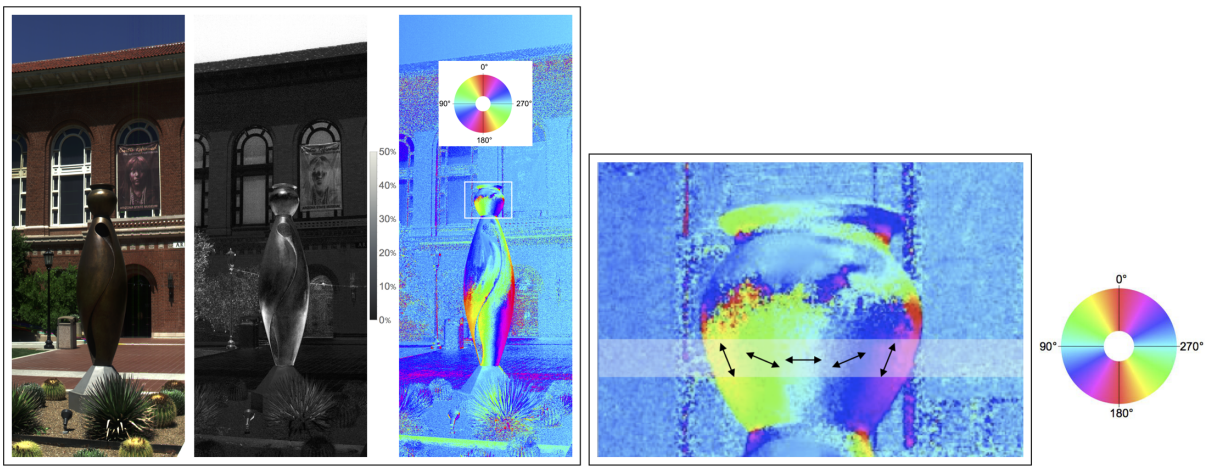

Fig. 3 (a) RGB radiance, DoLP, and AoLP$_m$ images of a metal sculpture with a spherical head that offers a range of surface orientations. (b) The polarization orientation on the statue's head is rendered in black arrows to show a trend tangential to the surface.

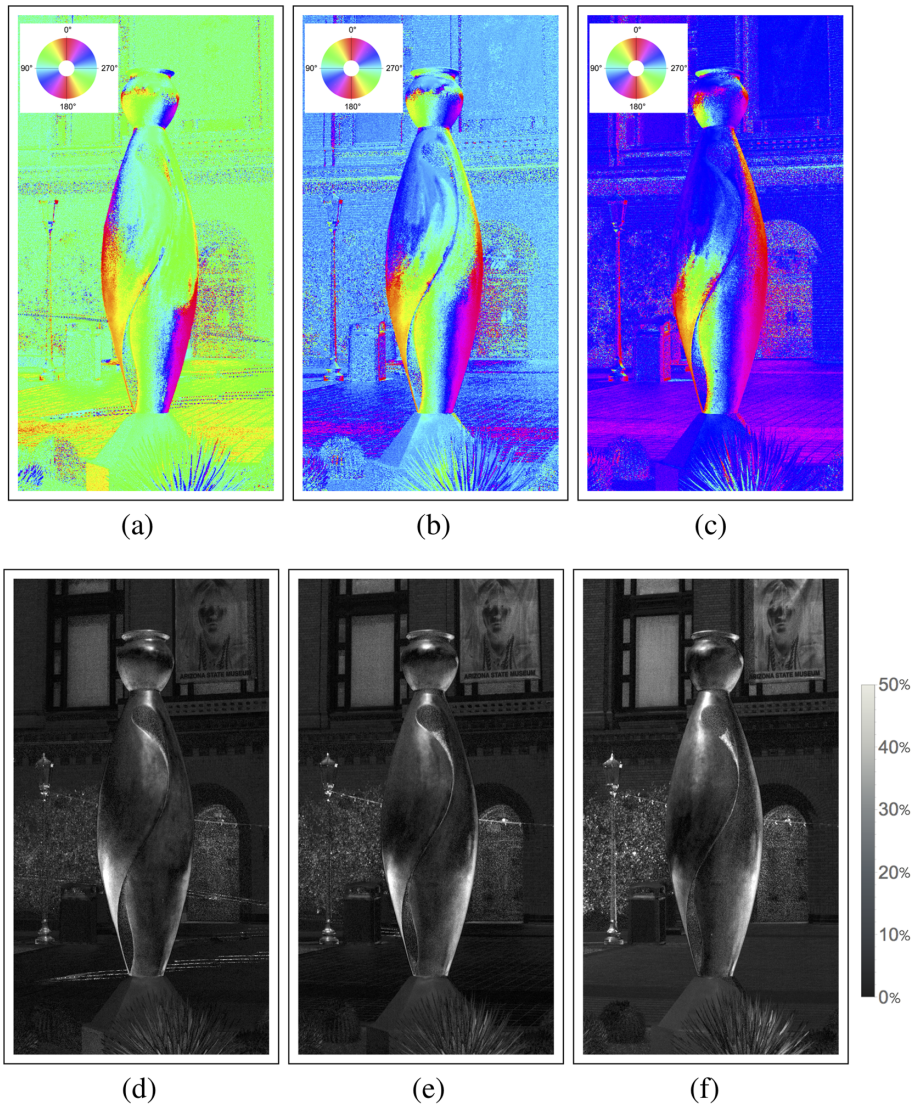

Fig. 4 AoLP$_m$ and DoLP images at three time points and therefore three scattering angles. AoLP$_m$ of the metal statue changes less throughout the day than rough surfaces such as the brick building, brick ground, and cement base of the sculpture. The only notable change in the DoLP at the different time points is the location of the bright sun-specular reflection on the top-half of the statue's head.

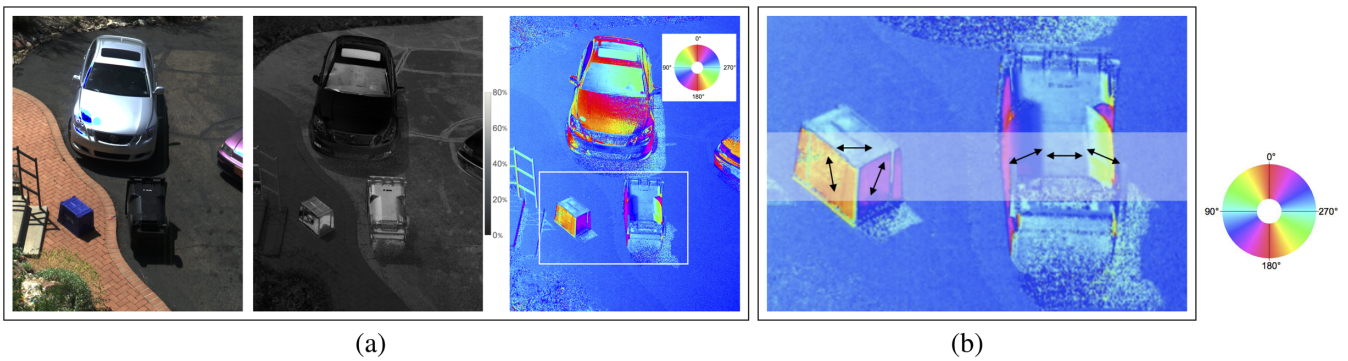

Fig. 5 A car, trash bin, and recycling bin in (a) RGB radiance, DoLP, and AoLP$_m$ images and (b) cropped to smooth plastic objects with polarization tangential to the surface rendered in black arrows to show tangential trend.

The relationship between AoLP and surface orientation of smooth objects also depends on if the dominant reflections are from the first surface of the material or if there is appreciable penetration depth, subsurface scattering, and refraction back out of the material.

4.2 *Relationship of Angle of Linear Polarization to Albedo*

The most well-known relationship between polarized light scattering and albedo is Umov's effect,[29] which states that the DoLP is inversely proportional to albedo. In other words, dark objects have a higher DoLP. This effect is attributed to a difference in the dominant scattering process of dark, as compared to highly reflective, objects. Multiple interactions are more depolarizing than a single reflection. The high albedo of white objects yields a larger fraction of multiple interactions in the reflected fields as compared to dark objects. Multiple interactions are extinguished by dark objects due to their low albedo. Figure 6(a) is an RGB image of two adjacent cars, one black and one white. Figure 6(b) shows the DoLP image, and the inverse relationship between albedo and DoLP is notable.

Umov's effect explains the change in the polarized light scattering processes that makes albedo and DoLP inversely related. Reflectance from low albedo objects is dominated by first surface reflections and high albedo objects yield relatively more multiple interactions. In this work, an effect between AoLP and albedo is observed. The explanation is similar to Umov's effect: a change in the polarized light scattering process for different albedos. The AoLPs on the roof of the black car and the roof of the white car are perpendicular to one another [see Fig. 6(c)]. The AoLP of the white car is perpendicular to the surface (i.e., *p*-polarized) due to its penetration into the material and refraction back out toward the camera. The black car polarized reflectance is due to single reflection off the top surface of the car and therefore the AoLP is parallel to the surface (i.e., s-polarized). An example of these different ray paths is depicted in Fig. 7. The low albedo of the black car results in high absorption and therefore low volumetric scattering. The surface reflections create polarized light reflected from the black

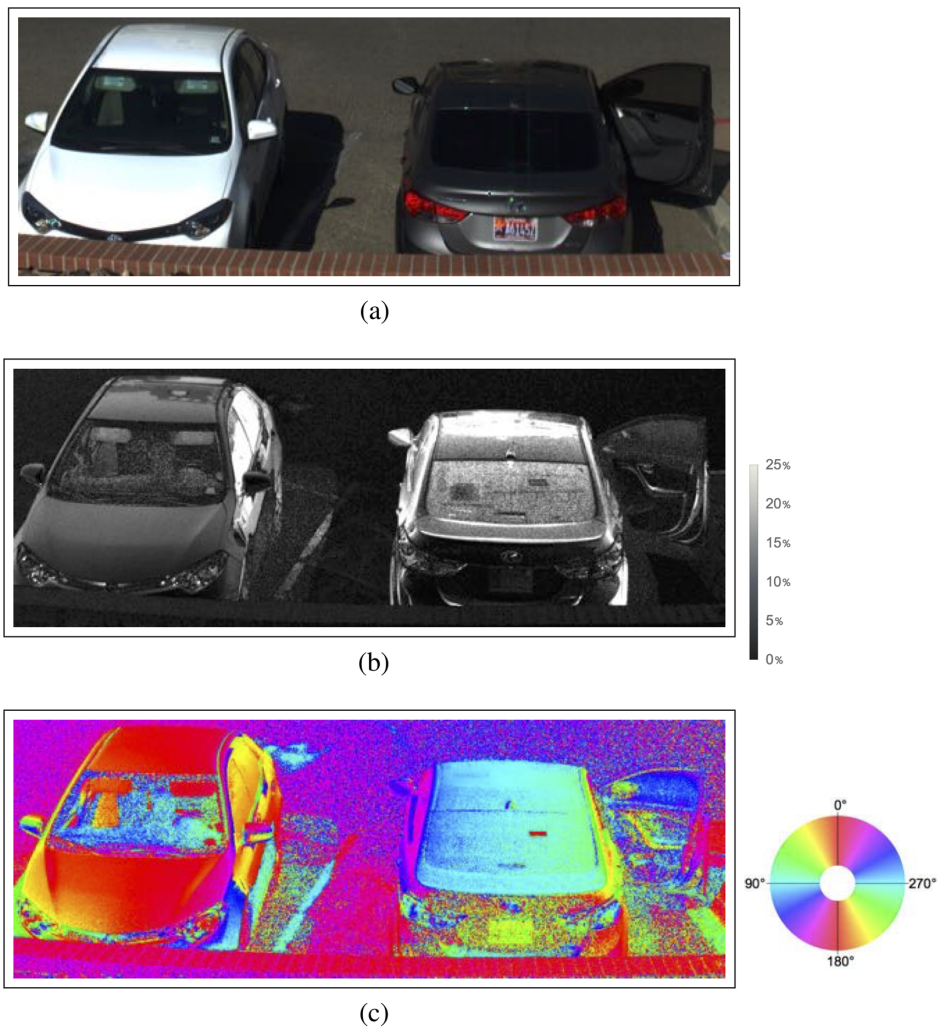

Fig. 6 Adjacent black and white cars in (a) RGB radiance, (b) DoLP, and (c) AoLP$_m$. The DoLP of the black car is greater than the DoLP of the white car as per Umov's effect. The AoLP of the black and white cars are perpendicular to one another due to the differences in albedo and associated dominant scattering processes.

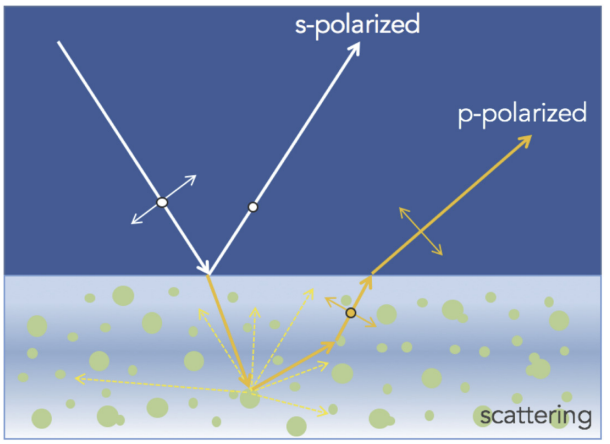

Fig. 7 The AoLP on the black and the white car roofs are perpendicular to one another [see Fig. 6(c)]. The AoLP of the white car is perpendicular to the surface (i.e., p-polarized) due to penetration into the material and refraction back out toward the camera. The black car polarized reflectance is due to single reflection off the top surface of the car and therefore the AoLP is parallel to the surface (i.e., *s*-polarized).

car. The high albedo of the white car results in low absorption and therefore higher volumetric scattering. The white car also reflects light from the surface but a larger contribution to the polarized reflectance comes from backscattered refraction. Light penetrates the surface of the white car, scatters within the material, and some of this scattered light is refracted back out of the material. Light becomes partially polarized when refracted. The two dominant scattering processes from the black and the white cars yield perpendicular polarization states: one from reflection from the car surfaces and the other from refraction. This relationship between the AoLP and the geometry of a car has been predicted in Ref. 1, although no dependence on the color of the car has been indicated. It is interesting to note that changing the sheen of the black paint on a car had no effect on the AoLP, as noted by researchers studying the behavior of polarization-sensitive insects who were attracted to the car surfaces.[30]

The albedo of a black and white car is both approximately spectrally invariant over the visible wavelength range. For many objects, including non-neutral colored cars, albedo is wavelength-dependent. Figure 8(a) is an RGB image of a red car. Figure 8(b) is the AoLP measurement for 470 nm (blue), and Fig. 8(d) is the AoLP measurement for 660 nm (red). Notice that the AoLP for 470-nm matches the black car condition. Here, the major contribution to polarization is due to first surface reflections since the 470 nm will be highly absorbed by the red car's paint pigment. The red wavelength matches an AoLP for high albedo surface types with high internal scattering like that of the white car. The AoLP on the hood of the car at 660 nm is close to perpendicular compared to the AoLP measured at the 470-nm wavelength. In other words, the AoLP on the hood of the car changes according to the albedo of the material at that wavelength. The trend between albedo and DoLP is predicted by Umov's effect: DoLP of 470 nm in Fig. 8(c) is higher than the DoLP of 660 nm in Fig. 8(e). The AoLP albedo dependence is only observed for direct solar illumination; the side of the car is in the shadow and the AoLP is the same over both wavelengths. The neutral-colored cars in the background do not have a spectrally dependent AoLP, even in direct illumination. This example demonstrates that the illumination, the albedo, and associated dominant scattering process need to be known to correctly interpret AoLP measurements and/or select an appropriate polarized light scattering model.

4.3 *Relationship of Angle of Linear Polarization to Illumination*

In the outdoor environment, the illuminating source can be any combination of sunlight, skylight, and radiation reflected from nearby objects. The white metallic dome of an observatory is measured on a cloudy day (Fig. 9) and on a sunny day (Fig. 10). Clouds are depolarizing over most scattering angles. Note that the DoLP of the sky on the cloudy day in Fig. 9(b) is close to 0, but the DoLP of the sky on the sunny day in Fig. 10(b) is close to 0.20. In both cases, the AoLP trends with the surface orientation of the dome but is flipped 90 deg when comparing sunny to cloudy conditions. This is an interesting special case of a white metallic object under two illumination conditions that each yields different dominant polarized light scattering. The illumination conditions on two different days causes a 90-deg flip of the AoLP measured from the white dome. In the car example the dominant scattering behavior changes when the illumination is constant but the albedo is different. On the sunny day, the image is acquired late in the day (see Table 1) and no sun-specular reflections on the dome are present. The remaining contribution to the reflected polarized radiance is from subsurface interactions and polarized light that is backscattered and refracted out of the surface (see *p*-polarized ray path in Fig. 7). This dominant scattering behavior is similar to the white car in Fig. 6. The dome and white car illuminated on the sunny day also radiate first surface reflections (see s-polarized ray path in Fig. 7). However, the high albedo of the material causes the backscattering term to dominate. On a sunny day objects are illuminated by two sources: direct solar illumination and scattered skylight. Direct solar illumination is several orders of magnitude greater than scattered skylight.[31] On the cloudy day (Fig. 9), direct solar illumination is blocked by the clouds and the dome is only illuminated by skylight. The dominant polarized light scattering is a specular reflection of the dome's surface toward the sky at all surface orientations. This dominant scattering behavior, i.e., first-surface reflections, is similar to the black car in Fig. 6 and creates the same AoLP trend with surface orientation.

There is a black metal door on the left-hand side of the building that is in the shade of a doorway. The DoLP of this object is high and it is vertically polarized on both cloudy and sunny days. By contrast, the AoLP values of the windows in this scene are flipped 90 deg on sunny versus cloudy days. There is a square window to the left of the dome and a taller window to the right of the dome that have an AoLP, which matches the left side of the dome on each day. These AoLP differences in Figs. 9 and 10 signify a difference in the dominant scattering process when the object is directly illuminated by the sun or in the shade (i.e., illuminated by skylight). This example shows that relatively ordinary changes in illumination can cause a large change in the dominant polarized light scattering process and AoLP.

The cloudy day dome measurement is also an excellent example of GroundMSPI's polarimetric accuracy. A white

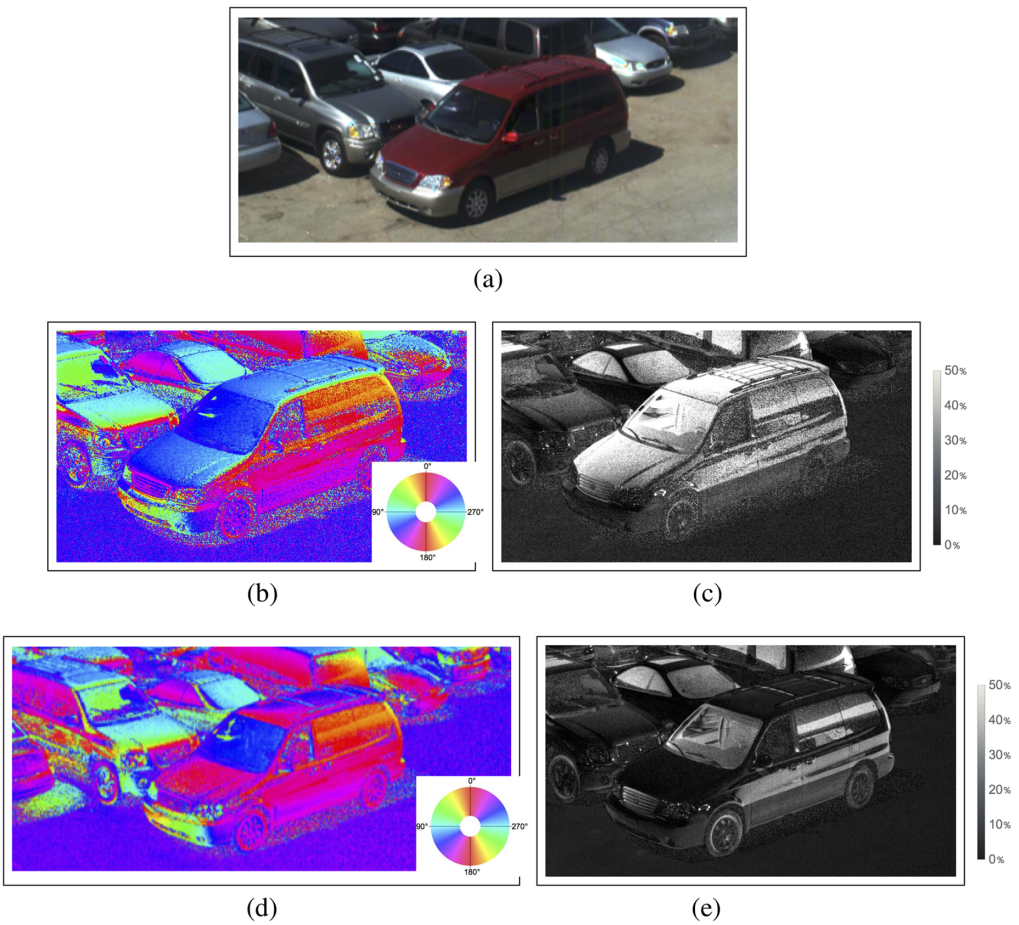

Fig. 8 Red car with neutral-colored cars in the background shown in (a) RGB radiance, (b)–(c) 470-nm AoLP and DoLP, and (d)–(e) 660-nm AoLP and DoLP. The AoLP of the red car's hood and roof at 470 nm is perpendicular to the AoLP at 660 nm due to differences in albedo and associated dominant scattering processes. The AoLP and DoLP values of the neutral-colored cars in the background are spectrally invariant compared to the red car.

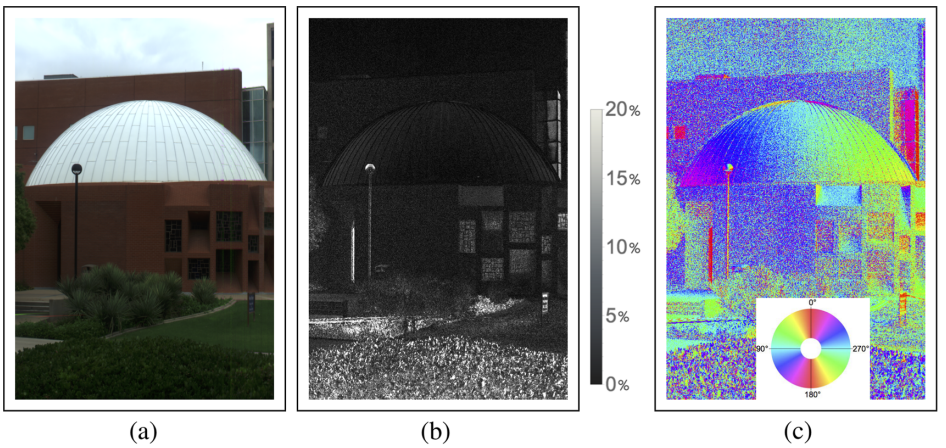

Fig. 9 On a cloudy day under diffuse illumination a white painted metal dome in (a) RGB radiance, (b) 660-nm DoLP, and (c) 660-nm AoLP. The DoLP ranges from 0.01 to 0.03 across the dome. The AoLP is perpendicular to the same object under sunny conditions reported in Fig. 10.

object is very depolarizing and on the cloudy day the DoLP in Fig. 9(b) is only 0.01 to 0.03 across the dome. The associated AoLP image in Fig. 9(c) still shows a clear trend with surface orientation even though this image looks noisier than Fig. 10(c) since the DoLP is higher on the sunny day.

Können's text on polarized light scattering in nature predicted and observed an AoLP tangential to the surface for

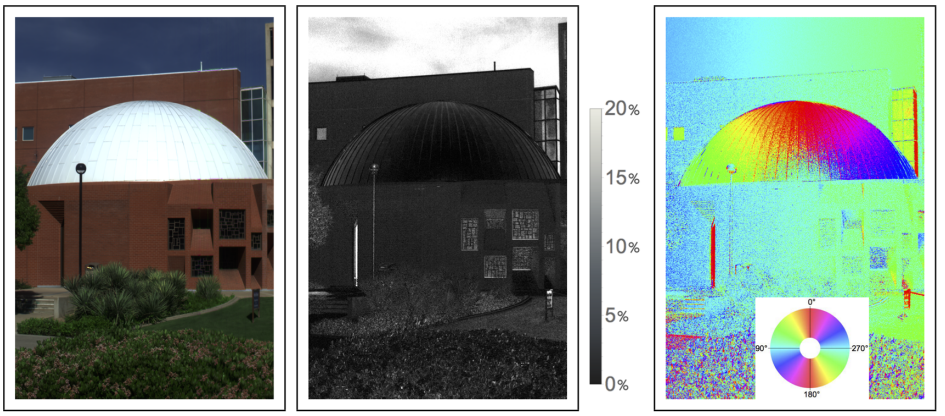

Fig. 10 On a sunny day under direct illumination a white painted metal dome in (a) RGB radiance, (b) 660-nm DoLP, and (c) 660-nm AoLP. The DoLP ranges from 0.07 to 0.08 across the dome. The AoLP is perpendicular to the same object under cloudy conditions reported in Fig. 9.

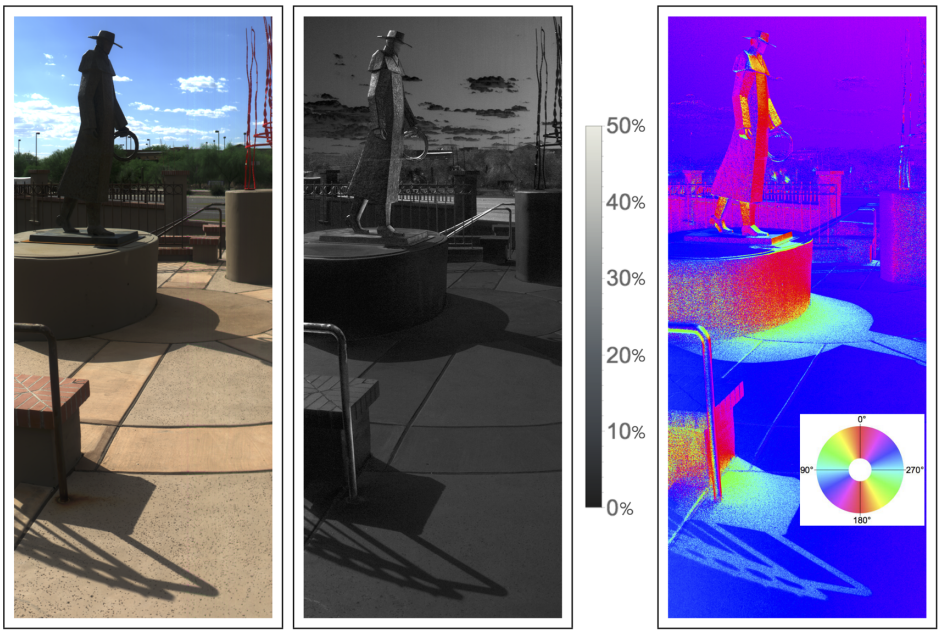

Fig. 11 A cement cowboy sculpture on a pedestal in (a) RGB radiance, (b) 660-nm DoLP, and (c) 660-nm AoLP$_m$. Notice the shadows on the pedestal and concrete ground. The AoLP in these shaded regions is tangential to the surface. A time-lapse movie (07:18 to 16:18 MST) is provided [Video 4, 17 MB, MOV (URL: https://doi.org/10.1117/1.OE.58.8.082419.4)].

objects in the shade.[1] Figure 11 illustrates this effect since the ground surface and perpendicular side of the pedestal are both in the shade. The AoLP in these two adjacent regions is tangential to each surface and perpendicular to each other. Where these regions intersect, at the bottom of the pedestal and ground next to the pedestal, the AoLP is shifted about 5 deg to 10 deg in these small regions toward the polarization orientation of the adjacent surface. This AoLP shift is likely due to reflections from the nearby surfaces. This effect is not observable when the two perpendicular surfaces are farther apart. Note that in Fig. 11(b) the cement ground does not match the AoLP of the sky. In this scene the sky contains clouds and therefore the sky AoLP is not expected to match a single-scattering Rayleigh model.[22]

5 Conclusions and Future Work

GroundMSPI AoLP observations have been related to surface texture, surface orientation, albedo, and illumination conditions. Most of these observations are consistent with the well-known principles of polarized light scattering. Owing to the high accuracy of GroundMSPI measurements, subtle changes in material properties and lighting conditions create interesting special cases, which have been described. Significant changes in the AoLP are caused by common

variations in outdoor illumination conditions. Also, simple variants in material properties change the dominant polarized light scattering process and thus the AoLP. Measurement examples that isolate a 90 deg AoLP flip are shown for a sunny day and a cloudy day as well as an object of high and low albedos. This flip is attributed to polarized light scattering, which is dominated by either (1) first-surface reflections or (2) transmission into the material followed by refraction out of the material. The higher absorption of a low albedo object prevents multiple interactions from backscattering inside the material followed by refraction out of the material. Polarized light scattering from both first-surface reflections and multiple interactions is present in the high albedo object. The 90-deg AoLP flip indicates that the contribution from multiple interactions dominates. The white dome imaged on a sunny day and a cloudy day also exhibits this 90-deg AoLP flip. In this example, the illumination, rather than material properties, has changed the dominate polarized light scattering path. On a sunny day, the dome is illuminated by two sources: direct solar illumination and scattered skylight; the former is greater than the latter by several orders of magnitude. On a cloudy day, the dominant polarized light scattering is a first-surface specular reflection of the dome's surface toward the sky. On the sunny day, the effect from direct solar illumination dominates. The AoLP is flipped 90 deg because it is transmitted into the material and refracted back out of the material.

Relating AoLP to surface properties requires prior knowledge about the dominant scattering processes and associated material properties and illumination conditions. A quantitative model to estimate surface orientation from imaging polarimetry would rely on this type of prior knowledge and require experimental validation.

In prior work, we estimated the surface orientation of rough materials from microfacet p-BRDF modeling.[15] These models predict an AoLP that is independent of wavelength, surface orientation, and acquisition geometry. Therefore, for these rough surfaces, the surface orientation estimates are derived from DoLP measurements at varying scattering angles.[6] Future work will include extending the estimation of surface orientation to materials that violate rough surface scattering models and study the sensitivity of these estimates to polarimetric measurements.

6 Appendix A: Appendix

The scattering plane contains the solar illumination vector and the view vector, which describe the direction that the camera is pointed. Often the instrument acquires images throughout the day while GroundMSPI's view direction remains constant. The illumination direction will vary, thereby changing the scattering plane. Figure 12(a) shows three example timestamps and their corresponding scattering planes as a red disk. The red arrow represents the illumination direction and the dark blue arrow represents GroundMSPI's pointing direction. The adjoining color circle represents the polarization orientation angles to the reference plane; red indicates the polarization orientation oscillating within the scattering plane and cyan is a perpendicular orientation to the scattering plane. Note that for the scattering plane case, the color wheel rotates with the illumination direction.

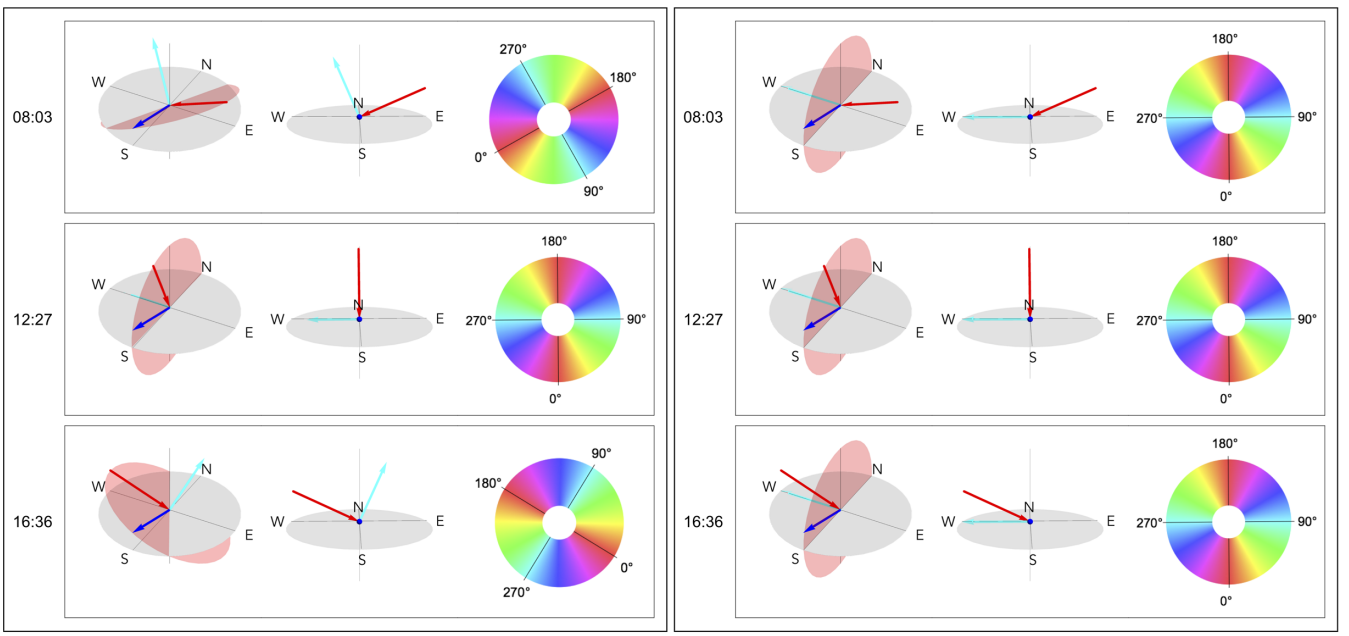

Fig. 12 Coordinate reference planes shown for (a) the scattering plane and (b) reference plane at three time points. Two views are provided to show the reference plane as a red disk, the solar illumination direction as red arrow, the view direction in dark blue arrow, and reference plane normal in cyan. The adjoining color circle represents the AoLP orientation to reference frames. The scattering plane is defined as the plane that contains the solar illumination direction and view direction. The scattering plane changes with illumination direction if view direction is held constant. The meridian plane is defined as the plane that contains zenith and view directions. If view direction is held constant, the meridian plane remains the same throughout the day.

The meridian plane shown in Fig. 12(b) contains the zenith direction and the view vector. This reference plane remains constant throughout the day since it does not depend on the solar illumination direction. For all three timestamps shown, the meridian plane and the adjoining polarization orientation color wheel remains constant since it does not depend on the solar direction and the view direction is constant.

Acknowledgments

This work was supported by the National Science Foundation under CHE-1313892 and by the National Aeronautics and Space Administration (NASA) Jet Propulsion Laboratories under University of Arizona subcontracts. The work by co-authors David J. Diner and Feng Xu were carried out at the Jet Propulsion Laboratory, California Institute of Technology under a contract with NASA.

References

1. G. Können, *Polarized Light in Nature*, CUP Archive (1985).
2. S.-M. F. Nee, "Polarization of specular reflection and near-specular scattering by a rough surface," *Appl. Opt.* **35**(19), 3570–3582 (1996).
3. L. B. Wolff and T. E. Boult, "Constraining object features using a polarization reflectance model," *IEEE Trans. Pattern Anal. Mach. Intell.* **13**(7), 635–657 (1991).
4. D. J. Diner et al., "First results from a dual photoelastic-modulator-based polarimetric camera," *Appl. Opt.* **49**(15), 2929–2946 (2010).
5. R. Walraven, "Polarization imagery," *Opt. Eng.* **20**(1), 200114 (1981).
6. L. B. Wolff, "Surface orientation from polarization images," *Proc. SPIE* **0850**, 110–121 (1988).
7. M. Kupinski, R. Chipman, and E. Clarkson, "Relating the statistics of the angle of linear polarization to measurement uncertainty of the Stokes vector," *Opt. Eng.* **53**(11), 113108 (2014).
8. D. Diner et al., "The Airborne Multiangle SpectroPolarimetric Imager (AirMSPI): a new tool for aerosol and cloud remote sensing," *Atmos. Meas. Tech.* **6**(8), 2007–2025 (2013).
9. D. J. Diner et al., "Joint retrieval of aerosol and water-leaving radiance from multispectral, multiangular and polarimetric measurements over ocean," *Atmos. Meas. Tech.* **9**(7), 2877–2907 (2016).
10. D. J. Diner et al., "Exploration of a polarized surface bidirectional reflectance model using the Ground-based Multiangle SpectroPolarimetric Imager," *Atmosphere* **3**(4), 591–619 (2012).
11. Y. Liu and D. J. Diner, "Multi-angle imager for aerosols a satellite investigation to benefit public health," Public Health Reports, 0033354916679983 (2016).
12. D. S. Saltzman et al., "Aerosol, cloud and ecosystems (ACE) proposed satellite mission," NASA, https://acemission.gsfc.nasa.gov/documents/Draft_ACE_Report2010%20.pdf (2010).
13. C. Bradley et al., "Spectral invariance hypothesis study of polarized reflectance with Ground-based Multiangle SpectroPolarimetric Imager (Ground-MSPI)," *Proc. SPIE* **9613**, 96130U (2015).
14. M. Kupinski and R. Chipman, "Power spectra trends in imaging polarimetry of outdoor solar illuminated scenes," *Proc. SPIE* **9853**, 98530O (2016).
15. M. Kupinski et al., "Applying a microfacet model to polarized light scattering measurements of the Earth's surface," *Proc. SPIE* **9613**, 96130T (2015).
16. H. Zhan et al., "Surface parameter based image estimation from application of a scattering model to polarized light measurements," *Proc. SPIE* **10407**, 104070U (2017).
17. M. Hamaoui, "Polarized skylight navigation," *Appl. Opt.* **56**(3), B37–B46 (2017).
18. J. Tyndall, "IV. On the blue colour of the sky, the polarization of skylight, and on the polarization of light by cloudy matter generally," *Proc. R. Soc. London* **17**, 223–233 (1868).
19. B. Suhai and G. Horváth, "How well does the Rayleigh model describe the e-vector distribution of skylight in clear and cloudy conditions? A full-sky polarimetric study," *J. Opt. Sso. Am. A* **21**(9), 1669–1676 (2004).
20. N. J. Pust and J. A. Shaw, "Digital all-sky polarization imaging of partly cloudy skies," *Appl. Opt.* **47**, H190–H198 (2008).
21. K. L. Coulson, "Polarization and intensity of light in the atmosphere," *Q. J. R. Meteorolog. Soc.* **116**(492), 521 (1990).
22. I. Pomozi, G. Horváth, and R. Wehner, "How the clear-sky angle of polarization pattern continues underneath clouds: full-sky measurements and implications for animal orientation," *J. Exp. Biol.* **204**(17), 2933–2942 (2001).
23. G. G. Stokes, "On the composition and resolution of streams of polarized light from different sources," in *Mathematical and Physical Papers*, Vol. **9**, p. 399, Transactions of the Cambridge Philosophical Society (1851).
24. T. W. Cronin and J. Marshall, "Patterns and properties of polarized light in air and water," *Philos. Trans. R. Soc. London Ser. B* **366**(1565), 619–626 (2011).
25. J. S. Tyo, B. M. Ratliff, and A. S. Alenin, "Adapting the HSV polarization-color mapping for regions with low irradiance and high polarization," *Opt. Lett.* **41**, 4759–4762 (2016).
26. F.-M. Breon et al., "Polarized reflectance of bare soils and vegetation: measurements and models," *IEEE Trans. Geosci. Remote Sens.* **33**(2), 487–499 (1995).
27. R. G. Priest and S. R. Meier, "Polarimetric microfacet scattering theory with applications to absorptive and reflective surfaces," *Opt. Eng.* **41**(5), 988–993 (2002).
28. N. J. Pust and J. A. Shaw, "Wavelength dependence of the degree of polarization in cloud-free skies: simulations of real environments," *Opt. Express* **20**(14), 15559–15568 (2012).
29. N. Umov, "Chromatische depolarisation durch lichtzerstreuung," *Phys. Z.* **6**, 674–676 (1905).
30. M. Blaho et al., "Unexpected attraction of polarotactic water-leaving insects to matt black car surfaces: mattness of paintwork cannot eliminate the polarized light pollution of black cars," *PLoS One* **9**(7), e103339 (2014).
31. J. E. Hansen and L. D. Travis, "Light scattering in planetary atmospheres," *Space Sci. Rev.* **16**(4), 527–610 (1974).

Meredith Kupinski is a research professor at the College of Optical Sciences, University of Arizona. She received her MS and PhD degrees in optical science from the University of Arizona in 2003 and 2008, respectively. Her research interests include task-relevant metrics for imaging systems design, estimation/detection theory, and stochastic systems analysis and information quantitation. She received NSF's Fellowship for Science, Engineering, and Education for Sustainability in 2013–2016.

Christine Bradley received her BS and PhD degrees in optical science and engineering from the University of Arizona, College of Optical Sciences, in Tucson, AZ, in 2011 and 2017, respectively. She is an optical engineer at the Jet Propulsion Laboratory, California Institute of Technology, with a focus on development of hyperspectral imaging instruments for Earth monitoring applications. Her current research also includes the development of reflection and diffraction models of roughened and smooth edges of a starshade for exoplanet research.

David Diner is a senior research scientist at the Jet Propulsion Laboratory, California Institute of Technology. He received his BS degree in physics from the State University of New York at Stony Brook in 1973, and his MS and PhD degrees in planetary science from the California Institute of Technology in 1977 and 1978, respectively. His research interests include atmospheric optics, remote sensing instrument development, multiangle and polarimetric observations of the atmosphere and surface, and aerosol impacts on air quality and climate.

Feng Xu received his PhD in physics from the University of Rouen (France) in 2007. He did his first postdoc research on light scattering by small particles at the Technical University of Darmstadt (Germany) from 2008 to 2009. In 2010, he joined the Jet Propulsion Laboratory (JPL) as a NASA postdoc program fellow to work on atmospheric radiation. Since 2013, he has been a research scientist with the Aerosol and Cloud Group working on remote sensing theory. He developed research algorithms to retrieve properties of aerosols over water, land, and clouds for JPL's Airborne Multiangle SpectroPolarimeter Imager (AirMSPI). He is currently responsible for developing an aerosol retrieval algorithm for NASA's Earth venture instrument, the Multi-Angle Imager for Aerosols (MAIA).

Russell Chipman is professor of optical sciences at the University of Arizona and a visiting professor at the Center for Optics Research and Education (CORE), Utsunomiya University, Japan. He received his BS degree in physics from MIT, and MS and PhD degrees in optical science from the University of Arizona. He is a fellow of OSA and SPIE and a coauthor of the textbook *Polarized Light and Optical Systems*. He received SPIE's 2007 G. G. Stokes Award for research in polarimetry and OSA's Joseph Fraunhofer Award/Robert Burley Prize for optical engineering in 2015.